

• Supplementary File •

# Trajectory-Free Dynamic Locomotion Using Key Trend States for Biped Robots with Point Feet

Lianqiang HAN<sup>1</sup>, Xuechao CHEN<sup>1,2\*</sup>, Zhangguo YU<sup>1,2\*</sup>, Xishuo ZHU<sup>3</sup>,  
Kenji HASHIMOTO<sup>4,5</sup> & Qiang HUANG<sup>1,2</sup>

<sup>1</sup>*School of Mechatronical Engineering, Beijing Institute of Technology, Beijing 100081, China;*

<sup>2</sup>*Key Laboratory of Biomimetic Robots and Systems, Ministry of Education, Beijing 100081, China;*

<sup>3</sup>*Intelligent Mine Research Institute, China Coal Research Institute Co., Ltd, Beijing 100013, China;*

<sup>4</sup>*Department of Mechanical Engineering Informatics, Meiji University, Kanagawa 214-8571, Japan;*

<sup>5</sup>*Humanoid Robotics Institute (HRI), Waseda University, Tokyo 162-8480, Japan*

## Appendix A Dynamic equation of model

We establish 7-DoF floating base dynamics for BR-S1, and define  $x_{\text{tor}}, z_{\text{tor}}$  as the position of the Center of Mass (CoM) for the torso,  $\theta_{\text{tor}}$  as the pitch angle relative to the vertical direction, and  $\theta_{\text{h}}^{\text{st}}, \theta_{\text{k}}^{\text{st}}, \theta_{\text{h}}^{\text{sw}},$  and  $\theta_{\text{k}}^{\text{sw}}$  the relative angles of the four joint-driven DoFs. The generalized DoF of model is  $q_w = [x_{\text{tor}} \ z_{\text{tor}} \ \theta_{\text{tor}} \ \theta_{\text{h}}^{\text{st}} \ \theta_{\text{k}}^{\text{st}} \ \theta_{\text{h}}^{\text{sw}} \ \theta_{\text{k}}^{\text{sw}}]^T$ . We can get the expression of the dynamics equation crossing to the Lagrange equation:

$$\begin{aligned} D(q_w)\ddot{q}_w + N(q_w, \dot{q}_w) &= B^T \tau + J_{\text{st}}(q_w)^T F_{\text{st}}^{\text{ext}} \\ \dot{J}_{\text{st}}(q_w)\dot{q}_w + J_{\text{st}}(q_w)\ddot{q}_w &= 0 \end{aligned} \quad (\text{A1})$$

where  $D \in \mathbb{R}^{7 \times 7}$  is the mass matrix,  $N \in \mathbb{R}^{7 \times 1}$  is the velocity product and gravitational term, and  $\tau \in \mathbb{R}^{4 \times 1}$  is the applied motor torque.  $J_{\text{st}} \in \mathbb{R}^{2 \times 7}$  is the combined support jacobian of the contact point,  $F_{\text{st}}^{\text{ext}} \in \mathbb{R}^{2 \times 1}$  is the ground reaction force.  $B \in \mathbb{R}^{4 \times 7}$  is the actuated joint selection matrix because there are only four joints to drive.  $\dot{q}_w$  and  $\ddot{q}_w$  are the first and second-order differentials of  $q_w$ , respectively. The external force  $F_{\text{st}}^{\text{ext}}$  is calculated by the linear acceleration at the CoM, because there is no torque constraint at the rear of leg. As  $F_{\text{st}}^{\text{ext}} = [F_c^x \ F_c^z]^T = [m\ddot{x}_C \ m\ddot{z}_C]^T$ .  $\ddot{x}_C$  and  $\ddot{z}_C$  are the x and z direction acceleration of the CoM, respectively.  $x_c^{\text{st}}$  and  $z_c^{\text{st}}$  are the x and z direction positions of the CoM relative to the contact point of the support leg, respectively.  $m$  is the total mass of the robot.

## Appendix B Whole body dynamic compensation: WBD-c

In order to control the robot to achieve the desired motion, the control quantity meets the characteristics of the mechanism. We propose a whole body dynamics compensation control method:

$$\ddot{\theta}_{\text{tor}}^{\text{ref}} = k_p^{\text{tor}}(\theta_{\text{tor}}^{\text{ref}} - \theta_{\text{tor}}) + k_d^{\text{tor}}(\dot{\theta}_{\text{tor}}^{\text{ref}} - \dot{\theta}_{\text{tor}}) \quad (\text{B1})$$

$$\tau_{\text{ff}} = B(D(q_w^{\text{ref}})\ddot{q}_w^{\text{ref}} + N(q_w^{\text{ref}}, \dot{q}_w^{\text{ref}}) - J_{\text{st}}^T F_{\text{ext}}) \quad (\text{B2})$$

where  $\ddot{\theta}_{\text{tor}}^{\text{ref}}$  is the reference angular acceleration of the torso pitch angle, which is related to the error of angle and velocity (Figure C1(iii)),  $\theta_{\text{tor}}^{\text{ref}}$  and  $\dot{\theta}_{\text{tor}}^{\text{ref}}$  are the reference angle and angular velocity of the torso, respectively.  $k_p^{\text{tor}}, k_d^{\text{tor}}$  is the stiffness of the spring and damping coefficient.  $q_w^{\text{ref}}, \dot{q}_w^{\text{ref}}, \ddot{q}_w^{\text{ref}} \in \mathbb{R}^{7 \times 1}$  are the reference position, velocity, and acceleration vector of the general coordinate system of the dynamic model of the floating base robot, respectively. Because of the nonlinearity of the dynamic inverted pendulum and the low-speed characteristic of the CoM in walking patten, the six quantities of the world coordinate system of the torso base  $x_{\text{tor}}^{\text{ref}}, z_{\text{tor}}^{\text{ref}}, \dot{x}_{\text{tor}}^{\text{ref}}, \dot{z}_{\text{tor}}^{\text{ref}}, \ddot{x}_{\text{tor}}^{\text{ref}}, \ddot{z}_{\text{tor}}^{\text{ref}}$  are ignored, and all of them are set to 0. The states of other joints are obtained by interpolation of driving points. During dynamic walking, the torso is expected to be vertical, so  $\theta_{\text{tor}}^{\text{ref}}, \dot{\theta}_{\text{tor}}^{\text{ref}}$  is also set to 0. The four  $\tau_{\text{ff}} = [\text{ff}\tau_{\text{h}}^{\text{st}} \ \text{ff}\tau_{\text{k}}^{\text{st}} \ \text{ff}\tau_{\text{h}}^{\text{sw}} \ \text{ff}\tau_{\text{k}}^{\text{sw}}]^T$  WBD-c torque values, which can also be called feed-forward torques, are obtained from the inverse dynamics. The reference acceleration of the CoM can be obtained through kinematics by using the given generalized DoFs acceleration reference value, to calculate the reference external force. The gravity at the center of mass is a constant value. The inverse dynamics is smoothed in  $n$  control periods after the change in leg state to avoid torque jumping. The calculation method of the  $j$  feedforward torque is  $\tau_{\text{ff}}^j = (\frac{n-j}{n})\tau_{\text{ff}}^{j-1} + (\frac{j}{n})\tau_{\text{ff}}^0$   $j \in [1, 2, \dots, n]$ .  $\tau_{\text{ff}}^0$  is the WBD-c torque value of the previous control cycle before the leg state is not switched. Since the inverse dynamic process is mainly calculated from the reference state, we call this method WBD-c.

Finally, to track the reference trajectory, a small gain parameter PD controller is used for joint torque control to generate the feedback control torque:  ${}^{\text{fb}}\tau_i^{\text{c}} = k_p^i(\varsigma\theta_i^{\text{ref}} - \varsigma\theta_i) + k_d^i(\varsigma\dot{\theta}_i^{\text{ref}} - \varsigma\dot{\theta}_i)$ .  $\varsigma\theta_i, \varsigma\dot{\theta}_i$  are the actual angle and angular velocity of the joint

\* Corresponding author (email: chenxuechao@bit.edu.cn, yuzg@bit.edu.cn)

for  $\varsigma$  states leg, respectively.  $k_p^i, k_d^i$  are the feedback coefficients of the PD controller. Based on the above, the feedback torque control vector  $\tau_{fb}$  is  $\tau_{fb} = [\text{fb}_{\tau_h^{\text{st}}} \text{fb}_{\tau_k^{\text{st}}} \text{fb}_{\tau_h^{\text{sw}}} \text{fb}_{\tau_k^{\text{sw}}}]^T$ . The final control torque for the robot consists of two parts:

$$\tau = \begin{cases} \tau_{ff}^j + \tau_{fb} & j \leq n \\ \tau_{ff} + \tau_{fb} & j > n \end{cases} \quad (\text{B3})$$

The control torque value is transformed into the current value  $I$  through the simplified relationship between the output torque and the current of the motor. Finally, the control of the required torque is achieved through the current loop of the driver.

## Appendix C Data analysis of robot experiment

To verify the effectiveness of the proposed method, a two-dimensional (2D), five-link, four-actuator planar robot with point foot called BR-S1 as shown in Figure C1b is developed by Beijing Advanced Innovation Center for Intelligent Robots and Systems, Beijing Institute of Technology. This style is very suitable for verifying the high dynamic motion theory and has been widely studied by researchers and used for algorithm verification [1]. Since the algorithm in the lateral plane is the same, the algorithm verification on the plane is applicable. However, considering the accuracy and flexibility of torque transmission, we adopt a belt wheel transmission with a low gear ratio and fix the robot in the 2D plane through the  $2m$  radial bar (shown in Figure C1a). The robot's motion track will be a circle with the fixed base as the center and the bar length as the radius. This bar limits the robot's motion in the x-z plane. The length of the radial bar is greater than the robot leg length ( $0.46m$ ), so that the influence of the height difference on the left and right legs is reduced. This scheme is often used in plane experiments and has little effect on the stability of the robot on the plane [2]. External Degrees of Freedom (DoF, Figure C1c) are used to measure the motion state of the robot such as position and velocity. The tibia is made of a hollow aluminum metal tube. At the end of the robot's foot, we use a bottom touch switcher instead of a force sensor to detect the contact state with the ground. Table C1 gives the dynamic parameters of the robot and the motion parameters of the driving joints.

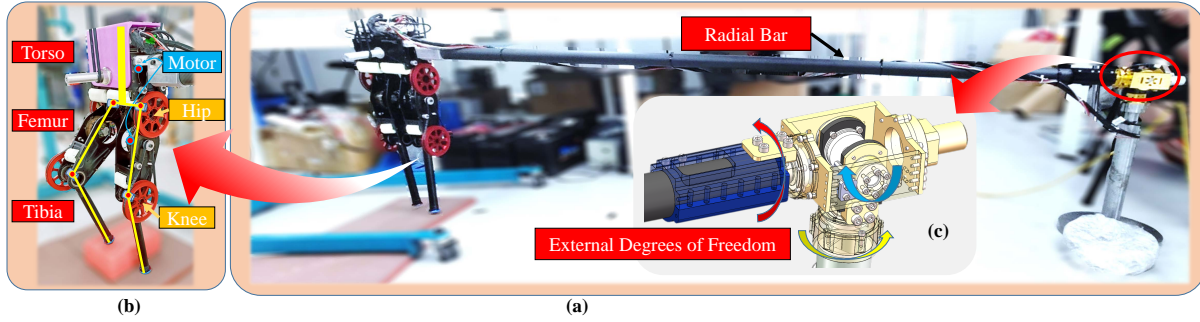


**Figure C1** BR-S1 robot experiment platform. (a) Panorama of RB-S1 robot experimental platform, (b) RB-S1 robot, (c) three degrees of freedom of radial bar configuration to assist in measuring position and orientation information of robot.

**Table C1** Dynamics parameters of robot body

Name	Mass(kg)	Length(m)	CoM(m) <sup>1)</sup>	Inertia(kg · m <sup>2</sup> )
torso	2.088	0.13	0.072(hip)	0.0044
femur	1.064	0.21	0.071(hip)	0.0038
tibia	0.329	0.25	0.041(knee)	0.0028
Name	Range(°)	Torque(N · m)	Belt ratio	Peak speed(rpm)
hip	-110 ~ 110	7.5	5	800
knee	-130 ~ 0	7.5	5	800

**Table C2** Definition of parameters used in experiment

Name	$\varsigma$	subp		$\text{subp}_{\varsigma} \theta_h^{\text{ref}}$		$\text{subp}_{\varsigma} \theta_k^{\text{ref}}$		$T_{\text{subp}}$	
$\Phi_{\varsigma}^s$	st	u		0.2rad		-0.3rad		0.2s	
		d		0.2rad		-0.3rad		0.1s	
	sw	u		0.45rad		-1.0rad		0.2s	
		d		0.17rad		-0.3rad		0.1s	
Gain	$k_d^{\text{sw}}$	$k_v^{\text{sw}}$	$k_p^{\text{h}}$	$k_d^{\text{h}}$	$k_p^{\text{k}}$	$k_d^{\text{k}}$	$k_p^{\text{tor}}$	$k_d^{\text{tor}}$	$n$
	0.5	0.3	4.2	0.5	2.9	0.1	195	17.4	50

1) Center of mass for rigid body part is relative to joint shown in brackets.

As shown in Table C2 is the KTS and feedback gain coefficient used in the experiment. Referring to the biped robot walking cycle of 0.4s and considering the leg length of BR-S1, we set the walking cycle time of 0.3s. we found that slow leg lifting can improve the stability of switching between support foot and swing foot, and fast foot landing can deal with large disturbance, so set  $T_d$  is 0.1s. The damping parameter of PD controller is about one tenth of the stiffness coefficient. The PD parameter used for joint angle control is not a high gain coefficient, which benefits from WBD-c. In the experiment, we perform a dynamic walking analysis and an anti disturbance data analysis to demonstrate the feasibility and robustness of our method. Meanwhile, the relationship between the feedforward torque and the PD control output in the joint torque control shows the importance of WBD-c. A computer with an Intel(R) Xeon(R) W-2145 CPU@2.70GHz was used as the robot computing platform.

### Appendix C.1 Stable walking gait of robot

Figure C2 shows the gait form in a three-step cycle when the robot is walking stably at a constant average speed. The hip joint track shows that the robot has a movement similar to an inverted pendulum, just like the supporting leg of a human. The angle between the torso and the vertical direction is controlled within the range of zero degrees, and the driving point of the hip joint and knee joint makes the swinging leg experience the process of raising a leg and stepping down with the real-time foothold adjustment. It can also be seen from the figure that the upper body leans forward for a short period after the legs are switched, and the swinging leg retracts. This unplanned and uncontrolled feature also helps the torso passively swing forward.

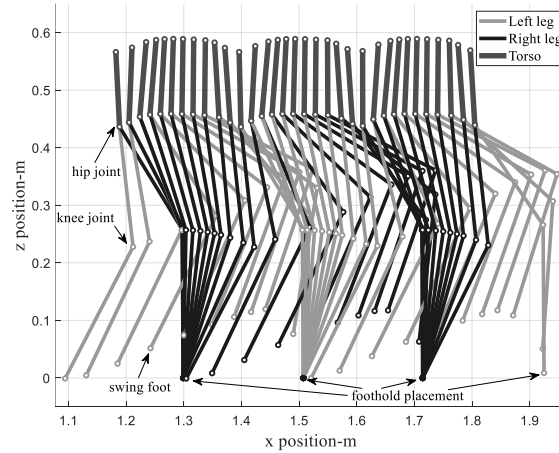


Figure C2 Angle limit cycles at different walking speeds in simulation.

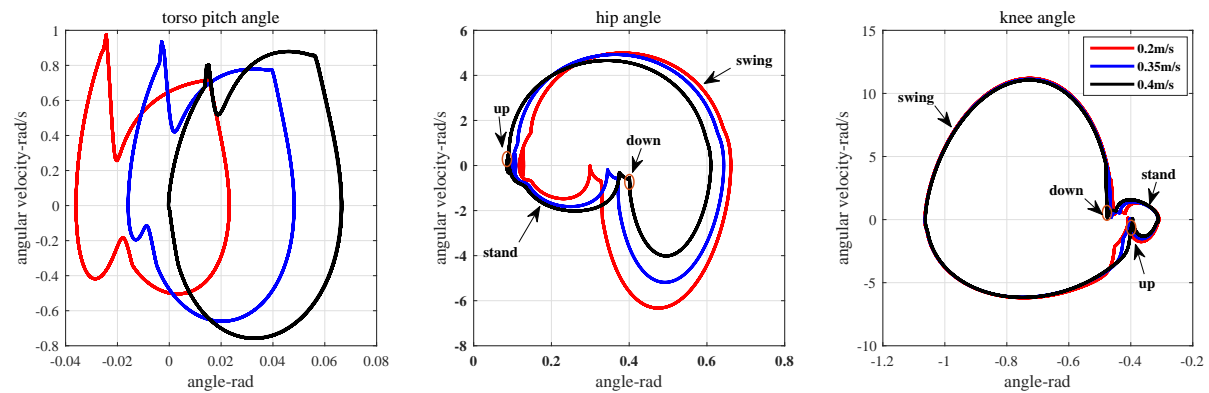


Figure C3 Angle limit cycles at different walking speeds.

### Appendix C.2 Gait at different speeds

Figure C3 shows the angle limit cycle of the robot walking stably at an average speed of 0.2m/s, 0.35m/s, and 0.4m/s. With an increase in speed, the trend of forward-leaning of the torso increased. This phenomenon is conducive to the maintenance of speed. The effect of increased speed on the knee joint is small because the adjustment algorithm does not directly affect the angle of the knee joint. By contrast, an increase in speed affects the trajectory of the hip joint. From the figure, we can see that the corresponding angle of the hip joint increases when it touches the ground. This is in line with the characteristics of real-time foothold adjustment and proves the effectiveness of the algorithm. Continuous limit cycles show the stability of the method presented in this paper.

### Appendix C.3 Experimental walking test

An experiment at a 0.5m/s walking speed was carried out on the RB-S1 robot platform (as shown in Figure C4). The bottom

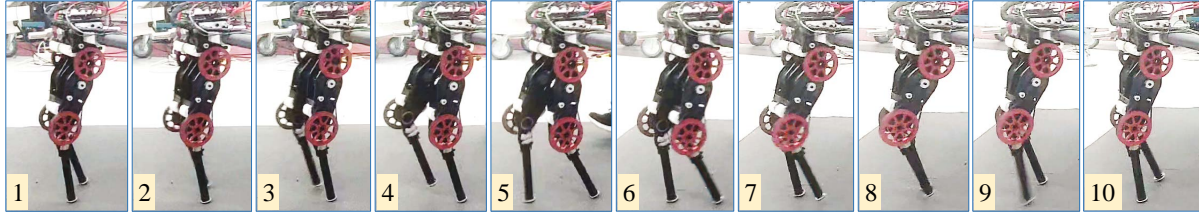


**Figure C4** Robot walked stably at average velocity of 0.5m/s. Screenshot shows two steps.

touch switcher can accurately detect the leg state, and the swing leg of the support leg can be successfully switched under control. The controller can operate at 1kHz. After an initialization phase of the robot, it is necessary to start from a standing step state, gradually increase the speed to a fixed speed, and then maintain stability (as shown in Figure C5). The figure shows the speed changes when walking; the speed stabilizes at 0.5m/s. Due to the velocity characteristics of the inverted pendulum, the actual velocity fluctuates slightly around the reference velocity. The experimental results show that the algorithm can run correctly within 1kHz control frequency, and KTS can complete the switching accurately. Compared with the off-line planning algorithm, the on-line real-time adjustment improves the mobility of the robot. For example, the speed and direction of the robot can be adjusted in real time.

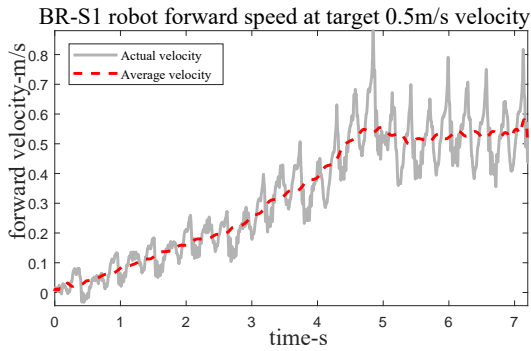


**Figure C5** Experimental data of robot's velocity. Solid line represents actual speed of robot's torso, and dotted line represents average change in speed.

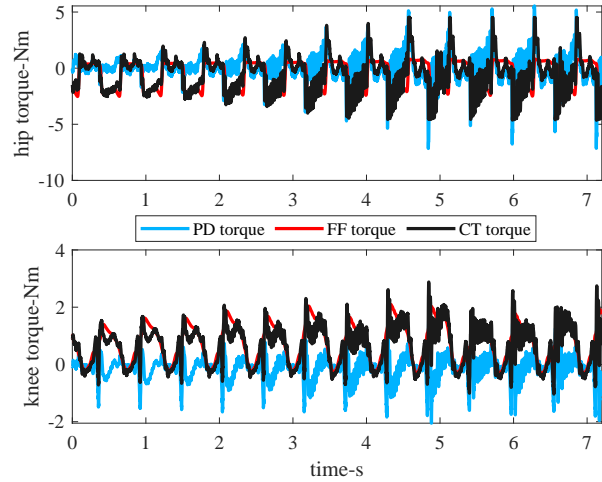


**Figure C6** Joint torque curve of robot while walking. FF torque is WBD-c torque calculated by torso attitude control algorithm, PD torque is adjusting torque of track following PD controller, and CT torque is total torque control quantity of joint.

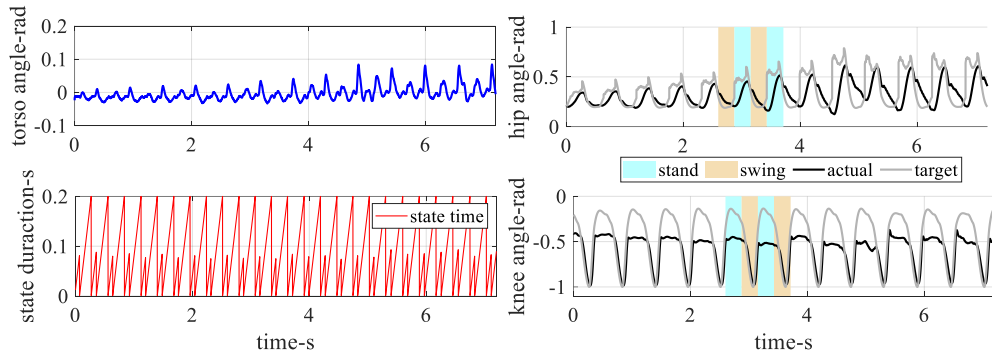


**Figure C7** Data analysis of robot walking stability experiment. Top left: changes in pitch angle of torso during walking. Right side: two images show angle changes of hip and knee joint of right leg, and shadow indicates current state of right leg. Lower-left: lifting and stepping time of swing leg in KTS.

In the walking data, as shown in Figure C7, the pitch angle of the torso is controlled at about zero degrees. The reference trajectory of the robot is the smooth trajectory of the driving point interpolation. It can be seen that the hip joint follows the

planning trend. With an increase in speed, the angle of the leg increases when the switch increases which shows the effectiveness of the adjustment of the foothold. Due to the lightweight of the lower leg, the tracking effect is good when swinging. The state durations show the single step cycle time. Because of the change of speed and the condition of event triggering, the lifting time of the swing leg is 0.2s. However, the stepping downtime does not reach the theoretical 0.1s, which indicates the importance of event triggering in leg switching. The tracking error of the joint trajectory does not affect the stability of the robot. This further proves the effectiveness of KTSs. The algorithm proposed in the paper is indeed trajectory-free. It is different from the traditional algorithm of accurately tracking motion trajectory.

The torque control quantity of the joint consists of the trajectory PD control and WBD-c torque of the torso attitude control. It can be seen from Figure C6 that the output of the control torque follows the WBD-c torque, and the PD controller adjusts it. The relation of driving torque composition shows the importance of feed-forward of WBD-c. With an increase in speed, the control torque increases but does not exceed the joint torque output range.

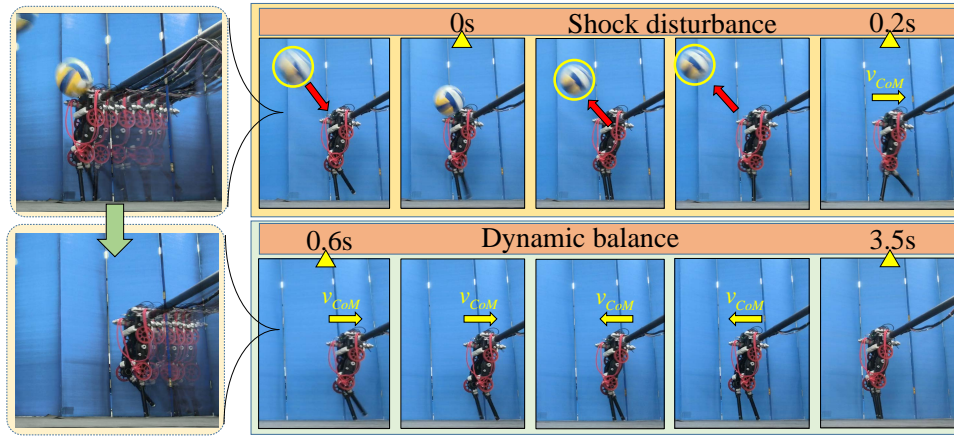


**Figure C8** Screen shot of robot's experiment after being hit by volleyball. After impact disturbance stage, robot enters dynamic balance stage to stabilize itself.

### Appendix C.4 Evaluation of robustness

The robustness of the algorithm is verified by experiments of uneven ground and shock disturbance. We used a volleyball weighing about 0.3kg to smash the robot's upper torso from a distance. Figure C8 is a screenshot of the stability of the robot after being disturbed. It takes about three seconds for the robot to return to a stable state, and thus the robustness of the algorithm is verified.

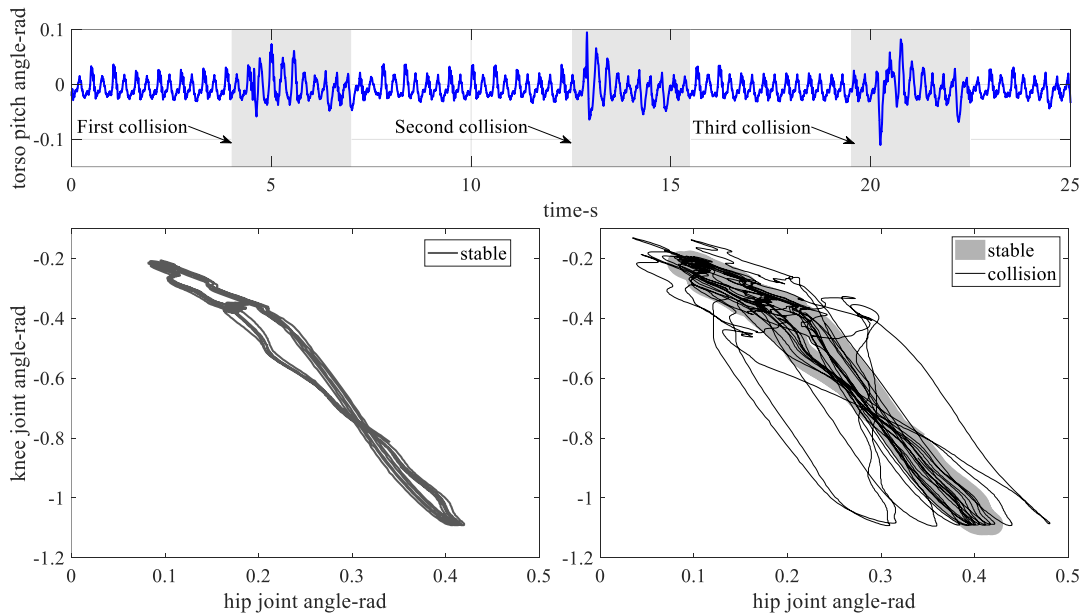


**Figure C9** Angle change of robot after being hit by volleyball in experiment. Top: change in pitch angle of torso; shadow area represents recovery process of robot after disturbance. Lower-left: relationship between hip joint and knee joint angle of right leg of robot in stable state. Lower-right: relationship between joint angle changes of robot after collision.

When the robot is hit by the volleyball (Figure C9), the maximum pitch angle of the torso can reach 0.1rad, which seriously affects the stable motion of the robot. Experiments show that the robot is stable again under the regulation of dynamic balance.

The relationship between two joints of the right leg is analyzed from the collision states. The image shows no obvious difference in the knee joint between the two states, but the range of the hip joint changes can reach 0.1 rad. This result further verifies the effectiveness and feasibility of the algorithm of adjusting the foothold by changing the angle of the hip joint.

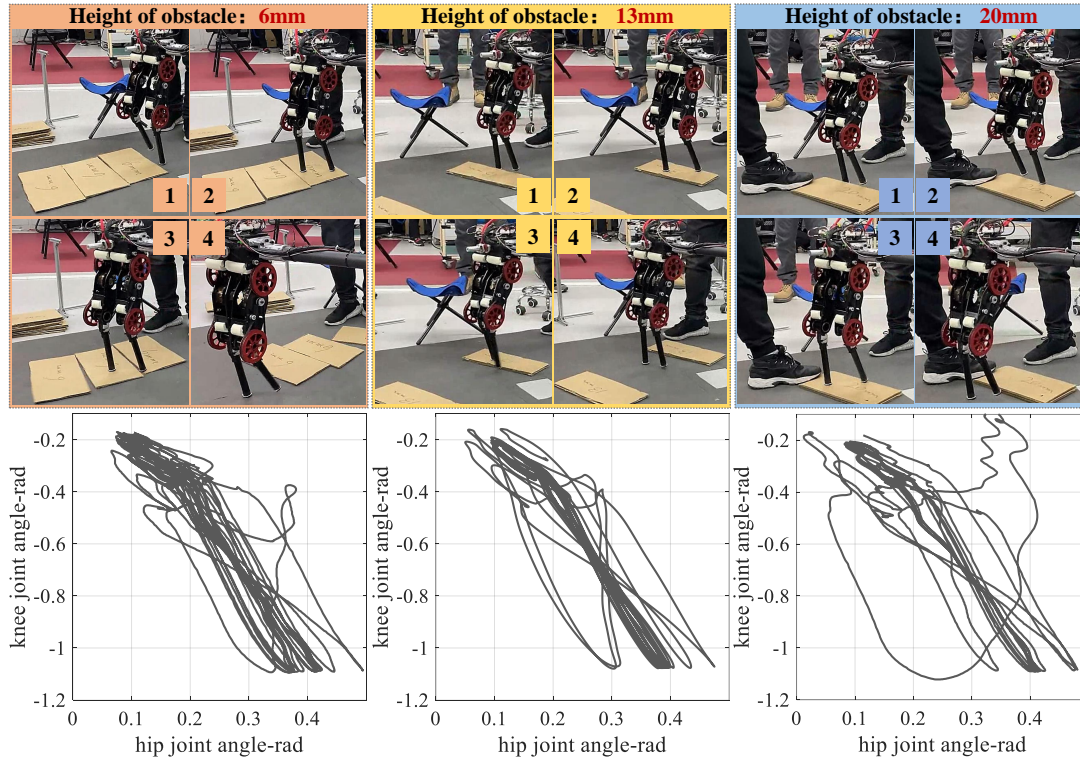


**Figure C10** Robustness test of walking on ground of different heights. Cardboard with height of 6mm, 13mm and 20mm is used to simulate uneven ground. The following three curves represent the joint trajectory relationship in the three terrain experiments.

In addition, as shown in Figure C10, we use cardboard of different heights to simulate uneven ground and to further verify the robustness of the algorithm. Due to the real-time adjustment of the foothold, the foothold in the current state can stabilize the robot, and the timely switching after landing enhances the robustness of the algorithm in advance. Through the relationship curve between hip and knee joint, it can be seen that with the increase of ground height, the adjustment of hip joint becomes larger and larger, so as to ensure the instability caused by external disturbance.

#### References

- 1 Fevre M, Goodwine B, Schiedeler J P. Terrain-blind walking of planar underactuated bipeds via velocity decomposition-enhanced control. *Int J Rob Res*, 2019, 38: 1307-1323
- 2 Martin A E, Post D C, Schiedeler J P, et al. The effects of foot geometric properties on the gait of planar bipeds walking under HZD-based control. *Int J Rob Res*, 2014, 33: 1530-1543